Configuration interaction approach to the few-body problem in a two-dimensional harmonic trap with contact interaction

M. Rontani,[1] S. Åberg,[2] and S. M. Reimann[2]

[1] *CNR-INFM National Research Center S3, Via Campi 213/A, 41100 Modena, Italy**

[2] *Mathematical Physics, Lund Institute of Technology, P. O. Box 118, 22100 Lund, Sweden*

(Dated: October 23, 2008)

The configuration interaction (CI) method for calculating the exact eigenstates of a quantum-mechanical few-body system is problematic when applied to contact interactions between the particles. In two and three dimensions, the approach fails due to the pathology of the Dirac δ-potential, making it impossible to reach convergence by gradually increasing the size of the Hilbert space. However, for practical applications this problem may be cured in a rather simple manner, by renormalizing the *strength* of the contact potential, which must be diagonalized in a *truncated* Hilbert space. The procedure relies on the comparison of CI energies and wave functions with those obtained by the exact solution of the two-body Schrödinger equation for the regularized contact interaction. The rather simple scheme, while keeping the numerical procedures still elementary, nevertheless provides both cut-off-independent few-body physical observables and an estimate of the error of the CI calculation.

PACS numbers: 67.85.-d, 31.15.ac, 34.50.Cx, 03.75.Ss

I. INTRODUCTION

Recent advances in the study of trapped ultra-cold atom gases [1, 2, 3] have put great emphasis on the key role of two-body interactions in a whole class of physical phenomena driven by particle-particle correlations [4]. Such systems represent an ideal laboratory for the investigation of many-body physics and the validation of many theoretical predictions. From the theory side, a major issue is the complexity of the atom-atom interaction potential, which can be hardly considered in full in theoretical simulations. On the other hand, very often only the low-energy scattering properties are relevant, which may be accounted for by simple model potentials. These model potentials may then be easily included e.g. in configuration interaction (CI) approaches to the few-body problem. The CI method displays unique features with respect to other numerical techniques, including an accurate treatment of correlation effects and access to both ground and excited states [5].

A most simple and yet useful model potential is the contact potential [6], which describes the s-wave isotropic scattering by means of only one parameter, i.e., the scattering length a. However, in connection with quantum mechanics the use of pointlike interactions is mathematically troublesome [7], as also noticed in studies of bosonic few-body systems [8]. The reader may find a brief history of contact potentials in Refs. 9, 10, 11, to mention just a few. A brief review of the current applications of contact interactions in the field of ultra-cold atom gases is for example found in the introduction of Ref. 12.

One major problem is that, in their simple form of Dirac δ-functions, contact potentials do not provide any scattering in two and three dimensions [6, 13, 14, 15, 16]. This problem may be solved by introducing a proper regularization, which slightly enlarges the Hilbert space spanned by the possible eigenstates of the Hamiltonian [6, 17]. This procedure, however, has subtle drawbacks, which are particularly relevant for the CI approach. The crux of the matter, as already noted by Huang [6], lies in the fact that the regularized operators may be non-Hermitian, which prohibits finding their eigenvalues by variational methods. In particular, the direct diagonalization of the Hamiltonian on a *complete* space provides only trivial (i.e., non interacting) solutions [6, 14], unless the class of allowed basis wave functions obey special (and often impractical) boundary conditions [16].

In this paper, we illustrate a rather simple alternative scheme to apply the CI method to the few-body problem with contact interactions. In a truncated Hilbert space, the coupling constant of the interaction potential is renormalized according to the energy cut-off considered in the calculation. This relation is established for the example of two particles confined in a two-dimensional harmonic trap, for which the exact regularized solutions are available [14]. We wish to point out that the CI diagonalization must be performed on a truncated Hilbert subspace. In fact, the ground-state energy obtained from the CI solution of the two-body problem has no lower bound as the size of the basis employed in the diagonalization increases. Similar results were already reported by Esry and Greene [16]. After truncation, the CI algorithm may *correctly* reproduce the exact energies and wave functions of both ground and excited states, except in a small range of the relative distance between the two particles, close to the origin. This agreement allows to map the coupling constant of the contact potential employed in the calculation to the two-dimensional scattering length a_{2D}. This mapping, however, significantly depends on the energy

*Electronic address: rontani@unimore.it; URL: www.nanoscience.unimo.it/max.html

cut-off.

In this paper, a relation between the coupling constant, the energy cut-off, and the scattering length is established, that straightforwardly may be used for CI calculations of few-body systems [18]. In spirit, this renormalization procedure is analogous to the ultraviolet renormalization adopted in similar contexts by means of diverse techniques, including space discretization [19], dimensional [11] and momentum-cutoff [11, 16, 20, 21, 22, 23] regularization, as well as to other approaches [24, 25, 26].

The structure of the paper is the following: After explicitely showing the failure of CI convergence in Sec. II, we discuss the exact solution of the two-body Schrödinger equation in Sec. III, which is based on the regularization of a pseudopotential operator. The key ideas are presented in Sec. IV, where we illustrate a successful strategy of comparing CI and exact results which provides a relation between the coupling constant of the contact interaction, the scattering length, and the energy cutoff of the calculation. After discussing the physical meaning of the truncation of the Hilbert space in Sec. V, we report the results of the renormalization procedure that are useful for actual CI calculations. Specifically, Sec. VI ilustrates CI results for the two-body problem in the relative-motion frame, which hold for both fermions and bosons, while Sec. VII considers the case of Slater determinants, which is the most relevant for applications to N fermions. Conclusions are drawn in Sec. VIII.

II. THE TWO-BODY PROBLEM IN A TWO-DIMENSIONAL TRAP: FAILURE OF CI CONVERGENCE

A simple, yet non-trivial example for investigating the nature of the contact interactions, is that of two interacting particles in a two-dimensional harmonic trap of characteristic frequency ω_0. Throughout this paper we use as energy unit $\hbar\omega_0$ and as length unit the oscillator length, $\ell_0 = (\hbar/m\omega_0)^{1/2}$. The two-body Hamiltonian, conveniently written in the center-of-mass and relative-motion coordinates $\boldsymbol{R} = (\boldsymbol{r}_1 + \boldsymbol{r}_2)/2$ and $\boldsymbol{r} = \boldsymbol{r}_1 - \boldsymbol{r}_2$, respectively, then reads as

$$H_2 = H_{\rm com} + H_{\rm rel}, \tag{1}$$

with

$$H_{\rm com} = -\frac{1}{4}\nabla^2_{\boldsymbol{R}} + R^2 \tag{2}$$

and

$$H_{\rm rel} = -\nabla^2_{\boldsymbol{r}} + \frac{1}{4}r^2 + g\delta(\boldsymbol{r}) \tag{3}$$

where g is the dimensionless coupling constant in units of $(\hbar\omega_0\ell_0^2)$.

The non-trivial part of H_2, $H_{\rm rel}$, pertains to the relative motion, while the center-of-mass eigenstates of $H_{\rm com}$ are simply Fock-Darwin orbitals in the $\boldsymbol{R}$ coordinate. The former may be solved by expanding the relative-motion wave function on a basis of Fock-Darwin orbitals [27]:

$$\Psi_m(\boldsymbol{r}) = \sum_{n=0}^{N_b-1} c_n\, \varphi_{nm}(\boldsymbol{r}). \tag{4}$$

Here the $\varphi_{nm}(\boldsymbol{r})$'s are the eigenstates of $H_{\rm rel}$ when $g = 0$, and N_b is the number of orbitals employed in the diagonalization. Moreover, if the relative-motion angular momentum is even (odd), the solution equally holds for spinless bosons and fermions with total spin zero (one). Here we investigate the lowest-energy singlet states of either two spinless bosons or two fermions of opposite spin 1/2. The eigenvalue problem consists in the diagonalization of the matrix

$$\langle n'|\, H_{\rm rel}\, |n\rangle = (2n+1)\delta_{n,n'} + \frac{g}{2\pi}, \tag{5}$$

where $|n\rangle = \varphi_n(\boldsymbol{r}) \equiv \varphi_{n0}(\boldsymbol{r})$ stands for the Fock-Darwin orbital in the $\boldsymbol{r}$-space with n nodes in the radial direction, $n = 0, \ldots N_b-1$, and $m = 0$, since the off-diagonal matrix element is zero for $m \neq 0$. The explicit orbital form is $\varphi_n(r) = (2\pi)^{-1/2} L_n(r^2/2) e^{-r^2/4}$, where $L_n(z)$ is the Laguerre polynomial of order n.

The ground state energy obtained from the numerical diagonalization of matrix (5) is plotted in Figs. 1 and 2 as a function of the basis size N_b, for several values of g, both for the repulsive (Fig. 1) and attractive (Fig. 2)

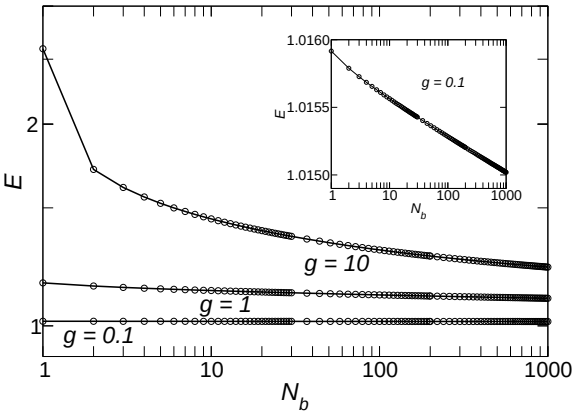

FIG. 1: Energy E of the two-body ground state in a two-dimensional harmonic trap vs number N_b of orbitals used in the CI expansion of the relative-motion wave function, plotted for different values of the coupling constant in the repulsive case, $g > 0$. Inset: same data for $g = 0.1$ with higher resolution of the energy scale. The energy unit is the spacing $\hbar\omega_0$ between oscillator shells. The center-of-mass contribution has been subtracted from the total energy, therefore in the absence of interaction $E = 1$.

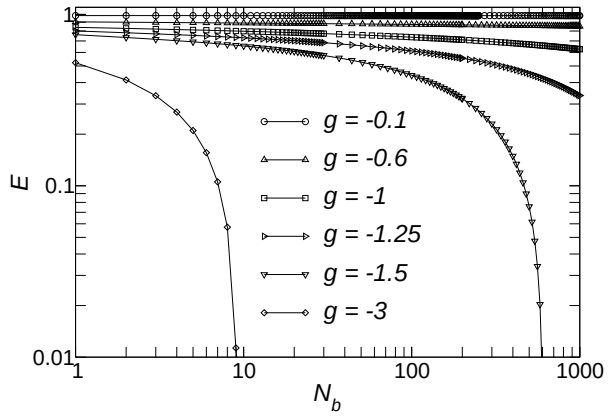

FIG. 2: Log-log plot of the energy E of the two-body ground state in a two-dimensional harmonic trap vs number N_b of orbitals used in the CI expansion of the relative-motion wave function, for different values of the coupling constant in the attractive case, $g < 0$. The center-of-mass contribution has been subtracted from the total energy, therefore in the absence of interaction $E = 1$.

case. From Fig. 1 (and the inset with higher resolution of the energy scale) it becomes apparent that the energy monotonously decreases as the basis size N_b increases, not indicating any convergence for the basis sizes at hand. The failure of convergence is dramatically evident for $g < -1$ (note the log-log plot of Fig. 2).

This incapability of reaching convergence over a finite Hilbert subspace could be expected also from the fact that the off-diagonal Hamiltonian matrix elements are independent from n [Eq. (5)]. Considering the case of large interaction strength $|g|$, the Hamiltonian can be approximately written in matrix form as $H_{\rm rel} \approx \boldsymbol{I} + g/(2\pi)\mathbf{1}$, where $\boldsymbol{I}$ is the identity and $\mathbf{1}$ is the $N_b \times N_b$ matrix with all elements equal to one. For large values of N_b the lowest eigenvalue is 1 and $-|g|/(2\pi)N_b$ for repulsive and attractive interaction, respectively, and it is clearly seen how the ground state energy diverges with N_b for attractive interaction [13]. This is also in agreement with the general expectation that the two dimensional Dirac δ-function does not provide scattering. Incidentally, we note that in the —well behaved— one-dimensional case the off-diagonal element is either zero or it decreases with n as $\sim (-1)^{(n+n')/2}(nn')^{-1/4}$.

III. THE EXACT SOLUTION OF THE TWO-BODY PROBLEM

An alternative approach to the solution of the two-body problem consists in introducing a properly regularized contact potential to replace the simple Dirac δ-function and then directly solving the Schrödinger equation. This path was successfully followed by Busch and coworkers [14], whose results we partly recall in this section referencing them as "exact". Later, Olshanii and Pricoupenko [28] provided a more general form of the pseudopotential, $V_{\rm pseudo}$, which should replace the simple Dirac δ-function in $H_{\rm rel}$,

$$V_{\rm pseudo} = -\frac{2\pi\delta(\boldsymbol{r})}{\log(\mathcal{A}a_{\rm 2D}\Lambda)}\left[1 - \log(\mathcal{A}\Lambda r)\frac{\partial}{\partial r}\right]_{r\to 0^+}, \quad (6)$$

where Λ is an arbitrary constant, $a_{\rm 2D}$ is the two-dimensional scattering length, $\mathcal{A} = e^{\gamma}/2$, and $\gamma = 0.5772\ldots$ is the Euler-Mascheroni constant. Here we express a few remarks which are relevant to the following application of the CI method.

The eigenstates of the regularized form of the relative-motion Hamiltonian, $H_{\rm rel}^{\rm reg}$, with

$$H_{\rm rel}^{\rm reg} = -\nabla_{\boldsymbol{r}}^2 + \frac{1}{4}r^2 + V_{\rm pseudo}, \quad (7)$$

are obtained by imposing that the wave functions, $\Psi(\boldsymbol{r})$, written as a linear superposition of Fock-Darwin orbitals $\varphi_n(\boldsymbol{r})$ with unknown coefficients c_n,

$$\Psi(\boldsymbol{r}) = \sum_{n=0}^{\infty} c_n\,\varphi_n(\boldsymbol{r}), \quad (8)$$

must solve the eigenvalue problem

$$H_{\rm rel}^{\rm reg}\,\Psi(\boldsymbol{r}) = E\,\Psi(\boldsymbol{r}). \quad (9)$$

The condition (9) together with the requirement of normalization allow to analytically determine both the coefficients c_n and the energy E, the latter through the equation

$$\psi(1/2 - E/2) = \log(2/a_{\rm 2D}^2), \quad (10)$$

where $\psi(z)$ is the digamma function of argument z [29]. The wave function is

$$\Psi(\boldsymbol{r}) \propto U(-\nu, 1, r^2/2)e^{-r^2/4}, \quad (11)$$

where $\nu = (E-1)/2$ and $U(a,b,z)$ is the confluent hypergeometric function. For details of the derivation see Ref. 14.

Figure 3 shows the ground state energy E as a function of $a_{\rm 2D}$, as obtained by solving Eq. (10). We here disregard the lowest-energy solution of Eq. (10) for $0 < a_{\rm 2D} < \sqrt{2}$, which is actually the true lowest-energy branch of the spectrum (not shown). The neglected branch refers to a deeply bound state whose energy indefinitely decreases as $a_{\rm 2D} \to 0^+$. The presence of such unusual bound state for repulsive interaction may be understood from the occurence of a pole in the upper plane of the complex wave vector of the scattering amplitude in free space, cf. Refs. 17 and 30. Throughout this paper we conventionally refer to the energy branch plotted in Fig. 3 as the lowest one. Such energy branch continuously evolves from the non-interacting ground state as $a_{\rm 2D}$ is varied, allowing for a one-to-one mapping between E and

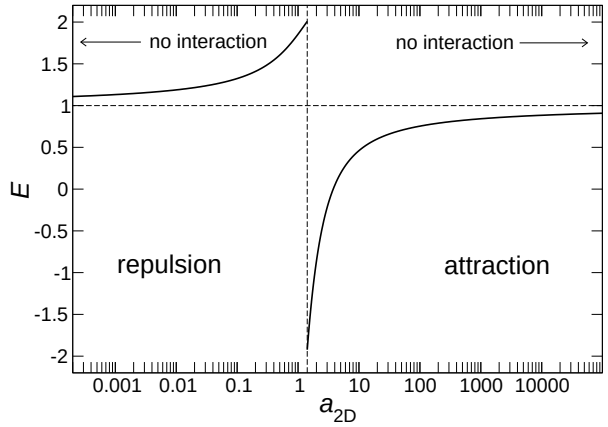

FIG. 3: Exact energy E of the two-body ground state in a two-dimensional harmonic trap vs scattering length a_{2D}. The center-of-mass contribution has been subtracted from the total energy, therefore in the absence of interaction $E = 1$ (dashed horizontal line). The dashed vertical line, for $a_{2D} = \sqrt{2}$, separates the branch for repulsive interaction ($E \to 1^+$ as $a_{2D} \to 0^+$) from that for attractive interaction ($E \to 1^-$ as $a_{2D} \to +\infty$). The energy unit is the spacing $\hbar\omega_0$ between oscillator shells and the length unit is the oscillator length, $\ell_0 = (\hbar/m\omega_0)^{1/2}$.

a_{2D} which will be extensively used throughout the paper. The energy E on the attractive side of the branch, for $\sqrt{2} < a_{2D} < +\infty$, is always smaller than the non-interacting value $E = 1$, which is smoothly reached as $a_{2D} \to +\infty$. For repulsion ($0 < a_{2D} < \sqrt{2}$), E is larger than the non interacting contribution $E = 1$, approached for $a_{2D} \to 0^+$.

In two dimensions, the interpretation of the scattering length is far from trivial: a_{2D} is always positive and the cross section diverges in the zero-energy limit. Specifically, we may understand the result of Fig. 3 that E approaches the non-interacting limit as $a_{2D} \to +\infty$, by recalling from scattering theory [31] that a_{2D} is the value of r for which the asymptotic form of the radial wave function $r^{1/2}\Psi(r)$ first becomes zero. In a short-range shallow attractive potential in three dimensions, the scattering length is negative for the lowest-energy scattering state, and it changes sign when the state becomes localized as the the depth of the potential increases. Exactly at the threshold depth, at which a bound state first appears, the scattering length diverges. This explains the resonant behavior of Fig. 3 ($a_{2D} \to +\infty$ as $E \to 1^-$), since in two dimensions any arbitrarily weak attractive potential admits a bound state with radius exponentially large in the binding energy [32]. As a_{2D} is decreased on the attractive side, the binding energy becomes stronger (E is reduced) as well as the typical radius of the bound two-body complex decreases. In free space, there would be no lower bound for the energy [30]. The effect of the confinement potential is such that, as the scattering length is further decreased and it becomes comparable to the radius of the trap, $a_{2D} \to \sqrt{2}$, the curve of the energy is folded into a different branch, which is actually the one we neglected. For further discussion see Refs. 30 and 34.

The key point in the derivation of Eq. (10) is that one is not allowed to interchange the limiting procedure contained in the definition (6) of $V_{\rm pseudo}$, $\lim_{r\to 0^+} \partial/\partial r$, with the infinite summation appearing in Eq. (8), $\sum_{n=0}^{\infty}$. In fact, by doing so, the "regularizing" part of the pseudopotential, $\lim_{r\to 0^+} \log(\mathcal{A}\Lambda r)\partial/\partial r$, provides a null result when applied to each addendum $\varphi_n(\boldsymbol{r})$ of the sum, which is well behaved at the origin. In this case, the only possible solution of Eq. (10) is the non-interacting one.

For the same reason, the regularization of $V_{\rm pseudo}$ is useless if the expansion (8) is finite, as it is of course the case for the CI algorithm. Thus, the regularization of the pseudopotential is irrelevant in this case. Equivalently, on any truncated Hilbert space, $H_{\rm rel}$ and $H_{\rm rel}^{\rm reg}$ of Eqs. (3) and (7) provide the same eigenvalues and eigenstates after the identification

$$g = -\frac{2\pi}{\log\left(\mathcal{A}a_{2D}\Lambda\right)}. \tag{12}$$

We conclude this section stressing that the physical observables of the two-body problem governed by $H_{\rm rel}^{\rm reg}$ do not depend on the numerical constant Λ appearing in the explicit form (6) of $V_{\rm pseudo}$, as it may be straightforwardly checked e.g. in the derivation of Eq. (10). This fact is also illustrated by the solution of the scattering problem in free space associated to $V_{\rm pseudo}$. From Appendix A one can see explicitely that the scattering amplitude does not depend on Λ as well as it coincides with the low-energy limit of any short-range potential.

IV. COMPARISON BETWEEN EXACT AND CI RESULTS

Let us now investigate whether it is possible to perform a CI diagonalization in a truncated Hilbert space, corresponding to a physically sensible cut-off, in order to obtain results which are nevertheless cutoff-independent. To accomplish this we suggest to employ the degree of freedom associated to the choice of Λ in the expression (12) for g in order to renormalize the coupling constant itself. The physical requirement validating the procedure is that one obtains the same CI energies and wave functions for different values of the energy cut-off, as well as that the CI data compare well with the exact results available for the two-body problem.

A. The two-body ground state

CI energies are obtained by performing the diagonalization by fixing the value of the coupling constant g. The result depends on the number N_b of orbitals used as a single-particle basis, as shown in Fig. 4. By using

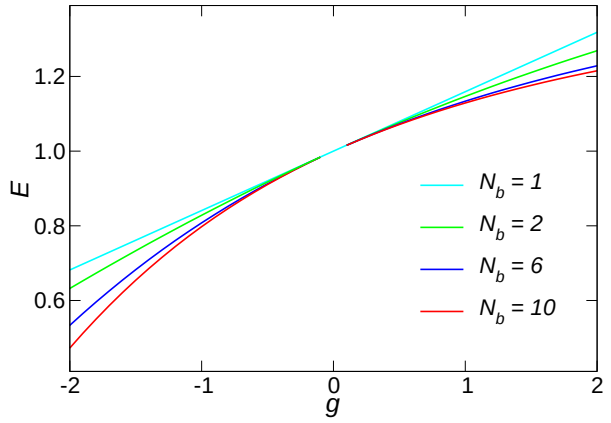

FIG. 4: (Colour) CI energy E of the two-body ground state in a two-dimensional harmonic trap vs coupling constant g, for different numbers N_b of orbitals used in the CI expansion of the relative-motion wave function. The center-of-mass contribution has been subtracted from the total energy, therefore for $g = 0$ —absence of interaction— $E = 1$.

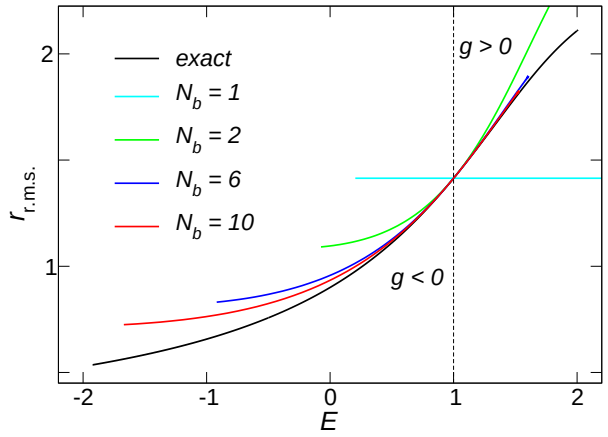

FIG. 5: (Colour) Root mean square radius, $r_{\rm r.m.s.}$, vs energy of the two-body ground state, E. Both exact (continuous black curve) and CI data (coloured curves) are displayed: the former are obtained by varying the two-dimensional scattering length, $0 < a_{\rm 2D} < \infty$ (cf. Fig. 3), the latter by varying the coupling constant, $-5 < g < 30$, for a given number of orbitals, N_b, used in the CI expansion of the relative-motion wave function (cf. Fig. 4). The black vertical dashed line is a guide for the eye: its intersection with the continuous black curve identifies the non-interacting ground state. CI data on the left (right) hand side correspond to attractive (repulsive) contact interaction. The center-of-mass contribution has been subtracted from the total energy. In the absence of interaction, the energy is $E = 1$ and the root mean square radius is $r_{\rm r.m.s.} = \sqrt{2}$.

just one orbital, $N_b = 1$, one recovers the result of perturbation theory at first order in g, therefore E depends linearly on g (cyan straight line in Fig. 4). By increasing N_b, E is reduced in a non-linear fashion, as it could be expected for a generic variational calculation (N_b in Fig. 4 increases by going from the green to the red curve). Since in the present case of contact interaction the diagonalization does not converge as N_b is increased, one needs to show that the same CI observables may be obtained for different values of N_b.

The first step in this empirical proof of principle is illustrated in Fig. 5, displaying the root mean square radius for the relative motion, $r_{\rm r.m.s.}$, as a function of the energy E of the two-body ground state. This is the simplest quantity providing information on the ground state wave function,

$$r_{\rm r.m.s.} = \left\{ \int_0^\infty dr \, |\Psi(r)|^2 \, r^3 \right\}^{1/2} \left\{ \int_0^\infty dr \, |\Psi(r)|^2 \, r \right\}^{-1/2} .$$

Obviously, repulsive (attractive) interaction implies an increase (a decrease) of both energy and radius with respect to the non-interacting values, $E = 1$ and $r_{\rm r.m.s.} = \sqrt{2}$, respectively. Figure 5 shows both exact and CI results: the possible ground states, represented in the $(E, r_{\rm r.m.s.})$ plane, form a geometrical locus parametrized by the allowed values of either the scattering length $a_{\rm 2D}$ for the exact case [black curve, cf. Fig. 3 and Eq. (10)], or the coupling constant g for the CI data (coloured curves, cf. Fig. 4). The black curve of Fig. 5 represents the exact data for the energy branch of the spectrum reported in Fig. 3, whose lower and upper bounds are $E = -1.923264$ and $E = 2.008166$, respectively. The coloured curves are obtained from CI diagonalization for a broad range of the coupling constant, $-5 < g < 30$. In Fig. 5, the non-interacting case is represented by the point of coordinates $(E, r_{\rm r.m.s.}) = (1, \sqrt{2})$, identified by the intersection of the vertical dashed line with the continuous black curve. The left (right) neighborhood of the non-interacting point corresponds to either the coupling constant $g \to 0^-$ ($g \to 0^+$) in the CI case (cf. Fig. 4), or the scattering length $a_{\rm 2D} \to +\infty$ ($a_{\rm 2D} \to 0^+$) in the exact case (cf. Fig. 3).

From Fig. 5 we see that all CI curves, shown for different values of N_b, remarkably overlap in some region of the $(E, r_{\rm r.m.s.})$ space, centered around the non-interacting point $(E, r_{\rm r.m.s.}) = (1, \sqrt{2})$. The actual range of the E-axis along which CI and exact data overlap depends on the values of both N_b and g: it is just the point $E = 1$ for $N_b = 1$ (cyan line), corresponding to the result of first-order perturbation theory that the wave function is not affected by the perturbation, and then it monotoneously increases with N_b up to a maximum interval approx. $0.5 < E < 1.5$ for $N_b = 10$ (red curve).

B. Two-body excited states

By comparing to the exact two-body solution [14], Fig. 5 in principle allows to estimate the relation between g and $a_{\rm 2D}$ once E and N_b are fixed, as well as to assess the error associated to the CI diagonalization. However, there is still some arbitrariness in the comparison be-

level	exact	CI	exact	CI
ground state	0.500	0.500	1.500	1.500
1st excited	2.613	2.619	3.596	3.608
2nd excited	4.647	4.657	5.658	5.688
3rd excited	6.666	6.680	7.706	7.757

TABLE I: Comparison between exact and CI energies for both ground and excited states, for attractive (2nd and 3rd column) and repulsive (4th and 5th column) interaction, respectively. Exact and CI data are linked by matching the ground state energies, providing $(a_{2D}, g) = (11.71, -1.855)$ and $(0.3294, 30.78)$ for $E = 0.5$, 1.5, respectively, where a_{2D} is obtained by solving Eq. (10) and g is obtained by diagonalizing Eq. (5) with $N_b = 13$. Excited state energies are then obtained by either solving Eq. (10) with a_{2D} fixed or by diagonalizing Eq. (5) with g fixed.

tween CI and exact data, since we could have chosen as well observables other than $r_{\rm r.m.s.}$ in order to characterize $\Psi(\boldsymbol{r})$. Therefore, as a second step of our proof of principle, in the following we straightforwardly compare both energies and wave functions of a few excited states. Such criterion is obviously much more stringent than the comparison of Sec. IV A.

As an example, we fix the CI basis size ($N_b = 13$) and consider two cases, corresponding to attractive and repulsive interaction, respectively. The corresponding values of the coupling constant g are obtained by matching the CI ground state energies with the chosen reference values. For $E = 0.5$ and $E = 1.5$ we obtain $g = -1.855$ and 30.78, respectively. By fixing g we compute CI energies and wave functions for the excited states, which are compared to the analogous exact quantities derived for fixed scattering length a_{2D} through Eqs. (10) and (11), respectively. The scattering length is deduced by solving Eq. (10) for $E = 0.5$ and 1.5, giving $a_{2D} = 11.71$ and 0.3294, respectively.

Table I compares energy levels up to the third excited state, showing that the worst relative error is 7 parts per thousand (for the 3rd excited level in the repulsive case). This very good agreement is confirmed by the wave function analysis, reported in Figs. 6(a) and (b) for attractive and repulsive interaction, respectively. The plots show the exact (red curves) and CI (black curves) radial probability densities of finding two particles at distance r, up to the third excited state. Such quantity, defined as $r\,|\Psi(r)|^2$ and normalized to one, allows to quantify the discrepancy between exact and CI predictions. We see in both attractive [Fig. 6(a)] and repulsive [Fig. 6(b)] cases that the overlap of the probability densities as well as the agreement regarding node locations is almost perfect far from the origin, becoming progressively worse as $r \to 0$. Such deviations, however, remain small in the whole range of r, so the overall matching between exact and CI results is excellent, consistently with the data of Table I. A closer inspection of the wave function behav-

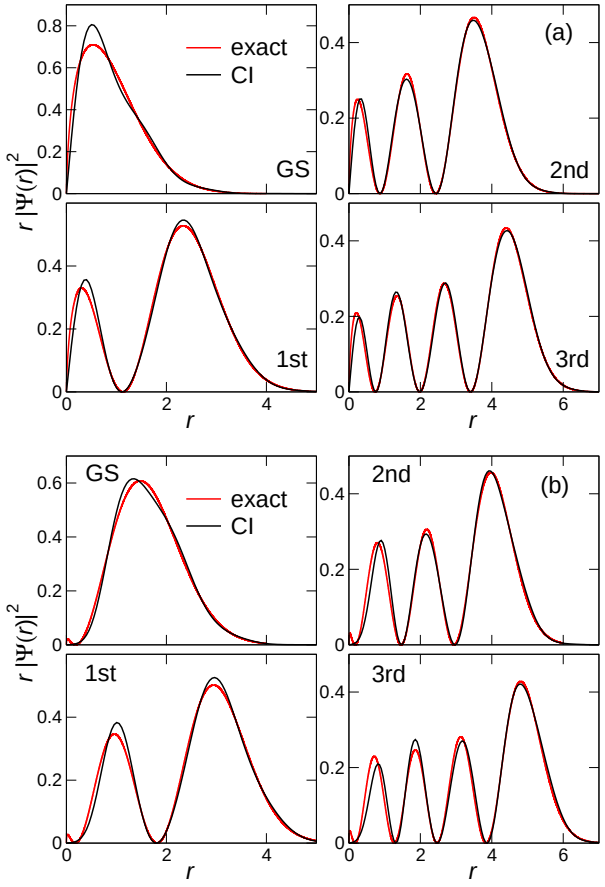

FIG. 6: (Colour) Radial probability density $r\,|\Psi(r)|^2$ of finding two particles at distance r, from both exact (red lines) and CI (black lines) calculations, for attractive (a) and repulsive (b) interaction, respectively. The panels display the ground (GS), first- (1st), second- (2nd), and third-excited (3rd) states obtained from both exact and CI calculations. Here $\Psi(r)$ is the relative-motion wave function normalized such that $\int dr\, r\,|\Psi(r)|^2 = 1$. For the exact calculations the values of $a_{2D} = 11.71$ and 0.3294 were used for attractive (a) and repulsive (b) interaction, respectively, while the coupling constant used in the CI diagonalization was $g = -1.855$ and 30.78, respectively, for a single-particle basis of $N_b = 13$ orbitals. The corresponding energies, up to the third excited state, are displayed in the 2nd and 3rd (4th and 5th) columns of Table I for attractive and repulsive interaction, respectively.

ior close to the origin, as discussed below, reveals significant qualitative differences between exact and CI results, which however do not affect the substantial agreement between wave functions in the whole space.

To summarize, we have shown so far that the CI method predicts energies and wave functions that compare well with the regularized ones, provided one works in a certain region of the $(E, r_{\rm r.m.s.})$ plane. This paves the way to the renormalization of the coupling constant g and to its actual usage in CI calculations. In the remaining part of the paper we will consider in detail such

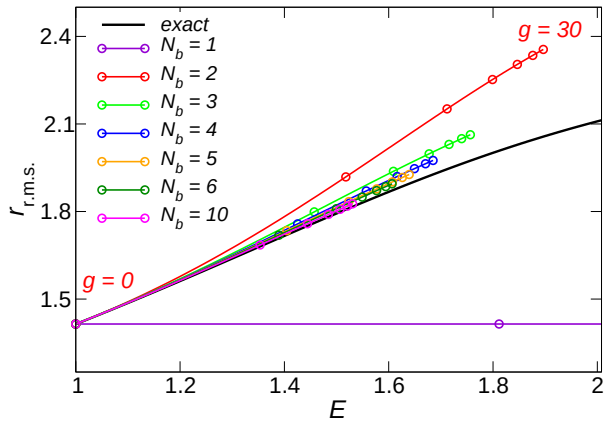

FIG. 7: (Colour) As Fig. 5 above, but zooming in on the region $1 < E < 2$. The separation between two consecutive circles in each CI curve corresponds to an increment of the coupling constant $\Delta g = 5$.

perspective.

V. ROLE OF CI TRUNCATION OF THE HILBERT SPACE

In this section we discuss the physical significance of the CI truncation of the Hilbert space. Going back to Figs. 4 and 5, we note that, once a positive (negative) value of g is fixed, the corresponding energy obtained through the CI method decreases when N_b increases. This may be seen in Fig. 5 e.g. from the displacement of the limits of the different CI curves for increasing values of N_b. Such limits correspond to $g = 30$ ($g = -5$) at the right (left) end of the curves. A magnification of Fig. 5 for a larger set of data in the region $g > 0$ shows that the scaling of E with g is non-trivial. In Fig. 7 the separation between consecutive circles in each CI curve corresponds to an increment in the g-space of $\Delta g = 5$. As g increases, the circles tend to cluster around a point of accumulation, i.e., the CI energy E tends to an upper bound as $g \to \infty$, the larger N_b, the smaller the limiting value. For $g < 0$, the situation is complementary (data not shown): $E \to -\infty$ as $g \to -\infty$, the larger N_b, the larger $|E|$. By extrapolating these results to the limit of completeness of the Hilbert space, $N_b \to \infty$, it is clear that $E \to 1$ for any fixed value of $g > 0$ and $E \to -\infty$ for $g < 0$. This behavior supports the fact that the contact interaction does not provide any scattering in the *free* two-dimensional space.

The above analysis for repulsive interactions implies that a truncated, smaller Hilbert subspace allows to access a broader range of the a_{2D}-space, which may be derived through Eq. (10) or Fig. 3 linking E and a_{2D}. However, this criterion must be balanced by the accuracy of CI energies and wave functions, which decreases with the size of the Hilbert space, as we now discuss.

N_b	$E = 0.5$ ($g < 0$)	$E = 1.5$ ($g > 0$)	$E = 1$ ($g = 0$)
2	1.58	3.54	1.41
3	1.21	2.57	1.08
4	1.00	2.14	0.912
5	0.86	1.86	0.803
6	0.77	1.67	0.726
10	0.53	1.21	0.552
13	0.41	0.99	0.481

TABLE II: Real-space cut-off, r_c, for a given number of Fock-Darwin orbitals, N_b, employed in the CI diagonalization of the two-body ground state wave function $\Psi_{\rm CI}(r)$ in the relative-motion frame of reference (see text). Data of second and third columns correspond to energies $E = 0.5$ and $E = 1.5$, being the largest roots of the equation $D(r_c) = D_{\rm threshold}$, with $D_{\rm threshold} = 0.02$ and 0.01, respectively. The last column reports the first zero of the N_bth non-interacting orbital along the radial direction as a reference.

In order to assess the accuracy of CI calculations, we define the real-space cutoff r_c as the lower bound of the interval $(r_c, +\infty)$ within which CI and exact wave functions overlap. Specifically, define the integral function $D(r)$ as the deviation of CI radial probability density $r\,|\Psi_{\rm CI}(r)|^2$ from the exact quantity $r\,|\Psi_{\rm exact}(r)|^2$, integrated from r to ∞:

$$D(r) = \int_r^{+\infty} dr' \left| |\Psi_{\rm CI}(r')|^2 - |\Psi_{\rm exact}(r')|^2 \right| r'. \qquad (13)$$

Since the wave functions are separately normalized to one, $0 \le D(r) \le 1$. Clearly, $D(r) \to 0$ as $r \to +\infty$ since the wave functions vanish at infinity. As r is reduced, $D(r)$ remains zero as long as $\Psi_{\rm CI}(r)$ and $\Psi_{\rm exact}(r)$ overlap. As r is further decreased, $\Psi_{\rm CI}(r)$ starts to deviate from $\Psi_{\rm exact}(r)$, so $D(r)$ reaches a global maximum at some finite value of r and then decreases again because $D(r) \to 0$ for $r \to 0$. We define r_c as the position at which $D(r)$ first assumes the value of $D_{\rm threshold}$ as r is reduced from infinity,

$$D(r_c) = D_{\rm threshold}. \qquad (14)$$

For given N_b, the value of g employed in the CI diagonalization is chosen such that the CI energy matches the reference value of the exact energy. This approach is the same as that used for Table I and Figs. 6(a) and (b). The values of r_c as a function of N_b for the ground states corresponding to the top left panels of Figs. 6(a) ($D_{\rm threshold} = 0.02$) and 6(b) ($D_{\rm threshold} = 0.01$), respectively, are collected in Table II. The value of r_c manifestly decreases as N_b increases, the larger $|g|$ the larger its magnitude. As a reference, we also report the first zero of the N_bth Fock-Darwin orbital along the radial direction, obtained as the smallest root of the equation $\varphi_{N_b-1}(r) = 0$. All the data show similar trends and may be fitted by a power law of the type $r_c \propto N_b^{\beta}$, where $\beta \approx -0.7$ for

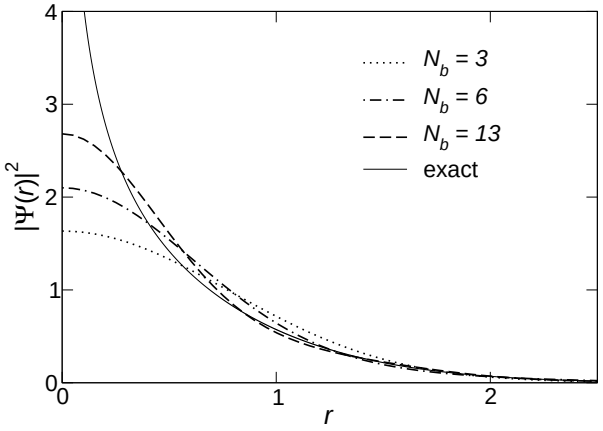

FIG. 8: Square modulus of the relative-motion wave function of the two-body ground state, $|\Psi(r)|^2$, vs radius, r, and as a function of the number of orbitals, N_b, used in the CI diagonalization. The value of the coupling constant, $g < 0$, for each subspace fixed by N_b has been chosen according to the renormalization procedure described in the main text. One finds g = -2.40, -2.10, -1.85, for N_b = 3, 6, 13, respectively. The continuous line is the reference square modulus of the exact wave function of the top left panel of Fig. 6(a), whose energy is $E = 0.5$. The wave function normalization is such that $\int dr\,|\Psi(r)|^2\, r = 1$.

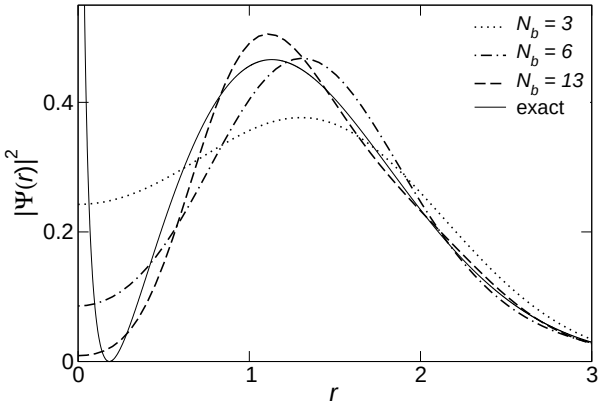

FIG. 9: Square modulus of the relative-motion wave function of the two-body ground state, $|\Psi(r)|^2$, vs radius, r, and as a function of the number of orbitals, N_b, used in the CI diagonalization. The value of the coupling constant, $g > 0$, for each subspace fixed by N_b has been chosen according to the renormalization procedure described in the main text. One finds g = 6.00, 10.0, 30.8, for N_b = 3, 6, 13, respectively. The continuous line is the reference square modulus of the exact wave function of the top left panel of Fig. 6(b), whose energy is $E = 1.5$. The wave function normalization is such that $\int dr\,|\Psi(r)|^2\, r = 1$.

$E = 0.5$ as well as for $E = 1.5$, and $\beta \approx -0.6$ for the non-interacting case. Therefore, since the value of N_b is the cut-off of the Hilbert space on the energy axis, E_c, and roughly $N_b \propto 1/r_c^2$, we may conclude that the cut-off values in real and energy spaces are complementary, $E_c \propto 1/r_c^2$. Here we assume that the cut-off values respectively in momentum space, p_c, and in real space, r_c, are related by $p_c \propto 1/r_c$.

It is also interesting to investigate in more detail the deviation of the CI wave function from the exact one close to the origin. To this aim we replace the plots of the radial density probability $r\,|\Psi(r)|^2$ of the top left panels of Figs. 6(a) and 6(b), respectively, with those of the square modulus $|\Psi(r)|^2$, shown as a function of r in Figs. 8 and 9, respectively. While the former is normalized to one and goes to zero as $r \to 0$, the latter may display possible singularities at the origin.

Figures 8 ($g < 0$) and 9 ($g > 0$) compare the exact wave function (continuous line) with those obtained by diagonalization for various basis sizes N_b. The square moduli of the exact wave functions present a logarithmic singularity at the origin, originating from the behavior of the hypergeometric function of Eq. (11):

$$\Psi_{\rm exact}(r) \approx \frac{A}{\Gamma(-\nu)}\left[\log r^2 + \psi(-\nu)\right] \quad \text{for} \quad r \approx 0,$$

where A is a normalization constant. Note the appearance of a node in the exact wave function of Fig. 9, due to the occurrence of a deeply bound state at much lower energy (cf. discussion in Sec. III). Any CI expansion of $\Psi_{\rm exact}(r)$ over a finite set of basis functions regular at the origin is unable to reproduce the logarithmic singularity, therefore any sensible comparison between CI and exact results must regard only the form of $\Psi_{\rm exact}(r)$ sufficiently far from the origin. On the other hand, as N_b is increased (going from dotted to dashed-dotted and dashed curves in Figs. 8 and 9), the overlap between exact and CI wave functions manifestly increases, as well as r_c diminishes, as shown in Table II. The presence of a singularity for $\Psi_{\rm exact}(r)$ is not important for practical calculations as long as its contribution to the radial density probability $r\,|\Psi_{\rm exact}(r)|^2$ is small, as demonstrated in Figs. 6(a) and 6(b).

The above scenario is implicit in the usage of the short-range pseudopotential as well, since that by definition is introduced in order to reproduce the asymptotic behavior of the scattering states (cf. Appendix A). On the other hand, similar concerns regard interaction potentials other than contact interactions. For example, CI diagonalizations employing simple orbital bases are unable to reproduce cusps in the wave functions originating from Coulomb interactions [33].

VI. RENORMALIZATION OF THE COUPLING CONSTANT

Let us now numerically investigate the functional relation between, on one side, the value of the coupling constant g and the size of the Hilbert space N_b actually employed in the CI diagonalization, and, on the other side,

the physical observable describing the short-range scattering, i.e., the two-dimensional scattering length a_{2D}, whuch is linked to the exact energy E via Fig. 3. This mapping may be seen as a renormalization of the coupling constant g through the free parameter Λ appearing in the expression (12), since the value of g corresponding to a certain value of a_{2D} depends on N_b as well.

The rather simple idea, based on the plots shown in Figs. 5 and 7, is now the following: The value of g to be linked to a certain value of the exact energy —say $\bar{E}$— is found by the intersection of the vertical line $E = \bar{E}$ with the CI curve corresponding to a given size N_b of the Hilbert space, since each point of the CI curve is associated to a specific value of g. The vertical distance between the CI and the exact black curve provides an estimate of the error of the CI calculation. Note that for two particles the value of E may be easily mapped to a_{2D} through Eq. (10).

Figures 10(a) and (b) for repulsive and attractive interactions, respectively, show the key results of the paper. The plots allow for identifying either the value of the two-body exact energy, E (left vertical axis), or, equivalently, the two-dimensional scattering length, a_{2D} (right vertical axis), as a function of the values of the coupling constant, g (horizontal axis), and of the size of the Hilbert space, N_b [coloured curves, going from $N_b = 2$ (orange) up to $N_b = 10$ (black)], employed in the CI diagonalization. The error associated to the comparison between CI and exact results is provided by the vertical error bars of the curves of Figs. 10(a) and (b). Such error is estimated as follows: From plots like Figs. 5 or 7 we associate to a given value of the energy, $\bar{E}$, a specific value of N_b and g: The latter is obtained by the intersection of the vertical line $E = \bar{E}$ with the CI curve for N_b. The vertical distance between the CI and the exact curve provides the error for $r_{\text{r.m.s.}}$, $\Delta r_{\text{r.m.s.}}$. Alternatively, from the intersection of the horizontal line $r_{\text{r.m.s.}} = \bar{r}_{\text{r.m.s.}}$ with the CI and exact curves, one could obtain an estimate for the error on the energy, ΔE. If the exact and CI curves are sufficiently close, we may assume that $\Delta r_{\text{r.m.s.}}/\Delta E \approx \partial r_{\text{r.m.s.}}/\partial E$, where the latter is the slope of the exact curve. Therefore, from the knowledge of both $\Delta r_{\text{r.m.s.}}$ and $\partial r_{\text{r.m.s.}}/\partial E$, one obtains the estimate for ΔE that is actually plotted in Figs. 10(a) and (b).

The main features of the plots are consistent with the findings of Sec. V. First, the accuracy of the calculation is maximum close to the non-interacting point, $g \to 0$, and it increases with N_b (the error bars are smaller if N_b is larger, once E is fixed). Second, if N_b increases, the energy depends more strongly on the strength of the contact interaction, g, for attractive interactions, while the opposite holds for repulsive interactions.

We would finally like to remark that the procedure reported in this section is similar in concept to the recent renormalized mean-field theory developed by von Stecher and Greene, where the scattering length used in a Hartee-Fock calculation is renormalized by mapping the self-consistent energy of two particles to the exact one [26].

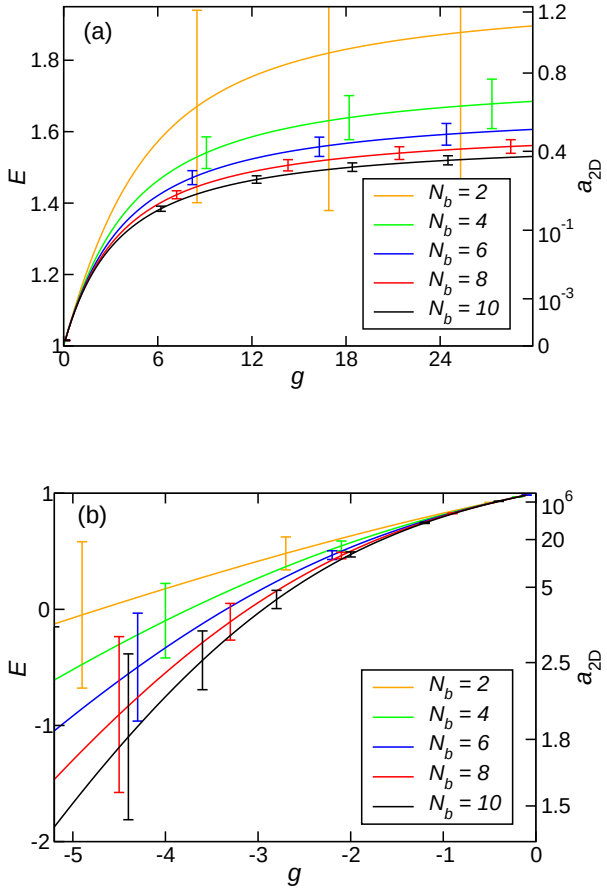

FIG. 10: (Colour) CI energy of the two-body ground state, E, vs. coupling constant, $g > 0$ (a) and $g < 0$ (b), for different numbers of orbitals, N_b, used in the CI expansion of the relative-motion wave function. The vertical error bars are estimated according to the procedure described in the main text. The right vertical axis shows the two-dimensional scattering length, a_{2D}, obtained through Eq. (10). The center-of-mass contribution has been subtracted from the total energy, therefore the non-interacting energy is $E = 1$.

VII. SLATER-DETERMINANT VS RELATIVE-MOTION BASIS

So far we have considered only two interacting particles, and for this special case we have uncoupled the relative motion from the center-of-mass oscillation. One of the advantages is that the results for two spin-1/2 fermions forming a singlet are the same as for two spinless bosons. However, for $N > 2$ this transformation turns out to be cumbersome for any efficient implementation of the CI algorithm. In fact, in typical codes, the N-body Hilbert space is spanned over a basis of either Slater determinants for fermions or permanents for bosons. It is therefore essential to verify that the results

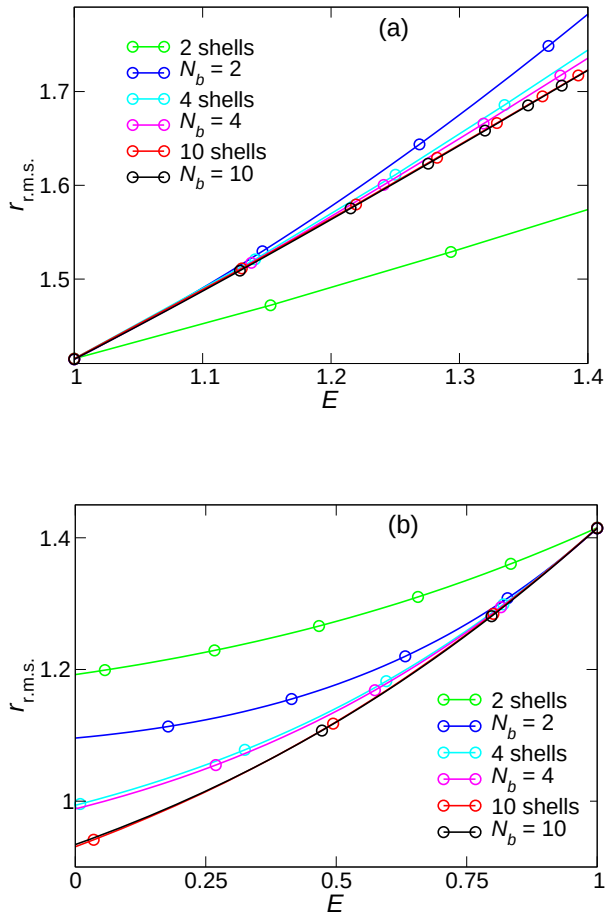

FIG. 11: (Colour) Root mean square radius, $r_{\rm r.m.s.}$, vs energy of the two-fermion CI ground state, E, computed by varying $g > 0$ (a) and $g < 0$ (b) in different Hilbert subspaces employed in the CI diagonalization. Green, cyan, and red curves are obtained from a Slater-determinant basis built including Fock-Darwin levels up to 2, 4, 10 energy shells, respectively. Blue, magenta, and black curves are obtained in the relative-motion frame, including up to $N_b = 2$, 4, 10 orbitals, respectively. The separation between two consecutive circles in each CI curve corresponds to an increment of the coupling constant $\Delta g = 1$, with $g \to 0^+$ as $E \to 1^+$ (a) and $g \to 0^-$ as $E \to 1^-$ (b). The center-of-mass contribution has been subtracted from the total energy. In the absence of interaction, $E = 1$ and $r_{\rm r.m.s.} = \sqrt{2}$.

reported in the previous sections still hold for these new bases.

To this aim we focus again on the case of two fermions. The Hamiltonian H_2 of Eq. (1), now written in terms of the standard coordinates $\boldsymbol{r}_1$ and $\boldsymbol{r}_2$, reads

$$H_2 = \sum_{i=1}^{2} \left(-\frac{1}{2}\nabla_i^2 + \frac{1}{2} r_i^2 \right) + g\,\delta(\boldsymbol{r}_1 - \boldsymbol{r}_2). \qquad (15)$$

In order to apply the renormalization scheme to a CI calculation performed on a basis of Slater determinants, we start again from the relation $r_{\rm r.m.s.}$ vs E (cf. Figs. 5 and 7). To evaluate the square modulus of the relative-motion wave function, $|\Psi(r)|^2$, needed to compute the root mean square relative distance, $r_{\rm r.m.s.}$, we first compute the pair correlation function $P(\boldsymbol{r}_1, \boldsymbol{r}_2)$:

$$P(\boldsymbol{r}_1, \boldsymbol{r}_2) = \frac{1}{N(N-1)} \sum_{i,j=1}^{N} \langle \delta(\boldsymbol{r}_i - \boldsymbol{r}_1)\delta(\boldsymbol{r}_j - \boldsymbol{r}_2) \rangle \,, \qquad (16)$$

where the average, $\langle \ldots \rangle$, refers to the CI ground state, and $N = 2$. By integration of $P(\boldsymbol{r}_1, \boldsymbol{r}_2)$ over the center-of-mass coordinate, $\boldsymbol{R}$, one is left with the probability density in the relative coordinate, $|\Psi(r)|^2$:

$$|\Psi(r)|^2 = 2\pi \int d\boldsymbol{R}\; P(\boldsymbol{r}/2 + \boldsymbol{R}, -\boldsymbol{r}/2 + \boldsymbol{R}), \qquad (17)$$

where $\Psi(r)$ is circularly symmetric.

Figures 11(a) and (b) compare the CI curves, $r_{\rm r.m.s.}$ vs E, for the two possible choices of the CI bases, either the Slater determinants (green, cyan, red curves) or the relative-motion Fock-Darwin orbitals (blue, magenta, black curves), in both cases of repulsive [$g > 0$, Fig. 11(a)] and attractive [$g < 0$, Fig. 11(b)] interactions, and for different basis sizes. Since a major purpose of the present scheme is the application to systems with $N > 2$, we limit ourselves to small basis sizes (maximum ten shells of Fock-Darwin orbitals). The CI code DONRODRIGO [35] was used for the calculation on the basis of Slater determinants. The conclusion one may draw from the plots is reassuring: while the results for the two bases significantly differ for excessively small sizes [cf. the blue and green curves for relative-motion orbitals ($N_b = 2$) and Slater determinants (two energy shells of Fock-Darwin levels), respectively], they tend to substantially coincide if the basis size is sufficiently large (e.g. $N_b \geq 4$ or more than four energy shells). Besides, a rule of thumb may be stated which connects the two bases: The CI diagonalization allows for essentialy the same results using either the Slater-determinant or the relative-motion bases, provided N_b equals the number of energy shells of Fock-Darwin levels which are filled in to build the Slater determinants. This is seen in Figs. 11(a) and (b), as the curves for the Slater-determinant and relative-motion bases — if matched according to the rule of thumb— tend not only to overlap as the basis sizes increase, but also to present the same dependence from g. The latter is given by the separation between two consecutive circles decorating the curves of Figs. 11(a) and 11(b), corresponding to the increment of the coupling constant $\Delta g = 1$.

The above rule of thumb may be explained as follows. The fact that the number of energy shells of Fock-Darwin levels must at least equal N_b is a necessary condition. In fact, the ground-state wave function, which is factorized into $\boldsymbol{r}$- and $\boldsymbol{R}$-dependent factors in the relative-motion frame, in the Slater-determinant space is built as superposition of products of two Fock-Darwin orbitals which depend on $\boldsymbol{r}_1$ and $\boldsymbol{r}_2$, respectively. Since Laguerre polynomials up to order $N_b - 1$, $L_{N_b-1}(r^2/2)$, span the $\boldsymbol{r}$-

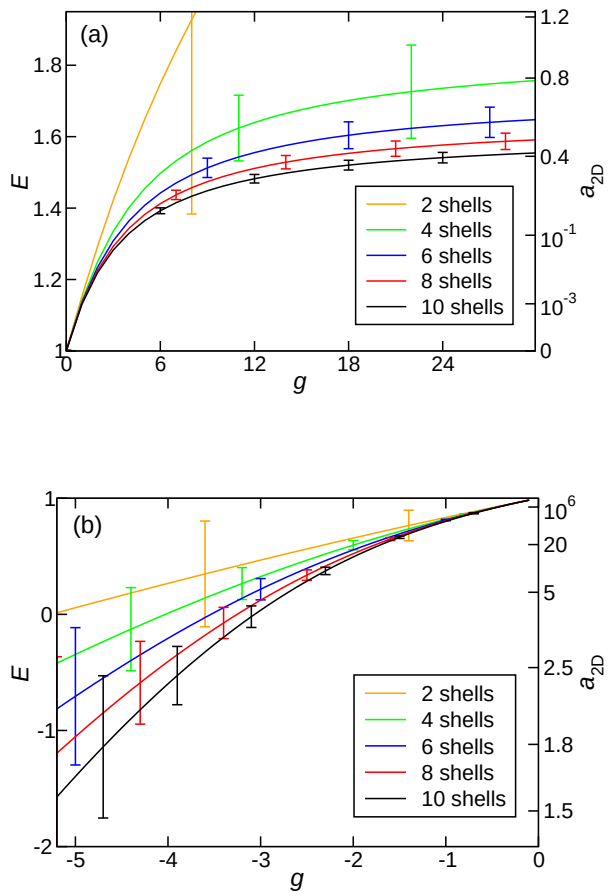

FIG. 12: (Colour) CI energy of the two-fermion ground state, E, vs. coupling constant, $g > 0$ (a) and $g < 0$ (b), for different numbers of energy shells of Fock-Darwin levels used in the CI expansion of the state over a basis of Slater determinants. The vertical error bars are estimated according to the procedure described in the main text. The right vertical axis shows the two-dimensional scattering length, a_{2D}, obtained through Eq. (10). The center-of-mass contribution has been subtracted from the total energy, therefore the non-interacting energy is $E = 1$.

dependent factor in the relative-motion frame, and because $L_{N_b-1}(r^2/2)$ is a polynomial of order $N_b - 1$ in r^2, then the $\boldsymbol{r}_1$- and $\boldsymbol{r}_2$-dependent Fock-Darwin orbitals must include powers of the radii, $r_1^{2\beta_1}$ and $r_2^{2\beta_2}$, respectively, at least of order $\beta_1 + \beta_2 = N_b - 1$. By considering only Fock-Darwin orbitals with zero azimuthal quantum number, $m = 0$, which typically provide the strongest contribution to the singlet ground state [36], the above constraint is enforced only if the number of energy shells is not smaller than N_b. With regards to the sufficiency of the rule of thumb, we note that, as the number of energy shells increases, the neglected high-energy contributions to the sum which gives $\Psi(r)$ gradually lose their relevance. Therefore, the usage of the two basis sets becomes essentially equivalent. Note that this same argument holds also for two bosons.

For the sake of completeness, in Figs. 12(a) and (b) we show the dependence of E (or a_{2D}) on g as computed from a CI diagonalization over a basis of Slater determinants. These curves should be directly compared with Figs. 10(a) and (b), obtained in the relative-motion framework. Since the plots in Fig. 12 provide information regarding the estimated error (vertical bars) associated to a given size of the Hilbert subspace (number of energy shells of Fock-Darwin levels), they are particularly useful for actual CI calculations. The detailed comparison between Fig. 12(a) [Fig. 12(b)] and Fig. 10(a) [Fig. 10(b)] confirms the rule of thumb: the curves are significantly different for small sizes of the diagonalization space [cf. the orange curves in Fig. 12(a) and Fig. 10(a)], while they tend to coincide as the size of the space increases, especially for repulsive interactions. For example, the asymptotic values of the blue, red, and black curves in Figs. 12(a) and 10(a) differ only for a few parts per thousand, and the differences become smaller as the basis size increases (from blue to black).

VIII. CONCLUSION

The aim of this paper is to provide a ground for CI calculations of N particles interacting via a contact potential. The configuration interaction method cannot be naively applied in two and three dimensions, due to the apparent pathology of the δ-function. To cure the problem for practical applications in a very simple and straightforward manner, we developed a procedure to renormalize the strength of the contact potential for two particles in a given subspace of single-particle basis states. The final outcome is that the CI diagonalization over a finite basis set provides physical observables whose values do not depend on the energy cut-off of the basis.

This procedure relies on the comparison of both the energy and wave function of two particles obtained by two different sets of data. The first set is computed by CI diagonalization with an energy cut-off, while the second one by the exact solution of the Schrödinger equation for the regularized form of the contact pseudopotential. Both ground and excited states are considered in this comparison. The analysis of CI data for a truncated Hilbert space provides a fully consistent physical picture of the results as well as a systematic assessment of the error of the calculation.

We believe this work allows for the application of the CI technique to the few-body problem with contact interactions. The interaction strength and model space of single-particle orbitals is defined from the investigation of the two-body problem and subsequently used for the N-body problem (see Ref. 18). It is natural to assume that the mapping between coupling constant, scattering length, and size of the Hilbert space for two particles, as reported in Figs. 10(a) and (b), as well as in Figs. 12(a) and (b), remains valid for $N > 2$, since the interaction affects pairs of particles while scattering events concerning

three and more particles are rare for sufficiently dilute systems. Besides, as N increases, the number of interacting pairs, $\approx N^2$, scales with N differently from the number of Slater determinants, $\approx e^N$ (provided the set of single-particle orbitals is fixed) [5]. We may therefore reasonably assume that our renormalization scheme is sound for $N > 2$, provided that the set of single-particle orbitals is sufficiently large. Nevertheless, if the set of orbitals is too small, the N-body Hilbert space could be artificially distorted (space filling effect).

In Ref. 18 we presented a first application of the method by studying the shell structure and the pairing of a few fermions in a two-dimensional trap. We expect that the present study paves the way to the *ab initio* investigation of few-body physics in cold atom traps.

ACKNOWLEDGMENT

This work is supported by CINECA-INFM Supercomputing Projects 2007 and 2008, by MIUR-FIRB Projects no. RBIN04EY74 and RBIN06JB4C, PRIN No. 2006022932, MAE Italy-Japan 2008, as well as NordForsk, the Swedish Foundation for Strategic Research, and the Swedish Research Council. We thank Daniela Pfannkuche, Chris Pethick, Ben Mottelson, Vladimir Zelevinsky, Pavel Kurasov, and Jonas Christensson for discussions.

APPENDIX A: SCATTERING AMPLITUDE FOR THE TWO-DIMENSIONAL REGULARIZED PSEUDOPOTENTIAL

In this appendix we derive the asymptotic form of the two-dimensional continuum states scattered by the regularized pseudopotential of Eq. (6), $V_{\rm pseudo}$, in free space. In the center-of-mass framework, the problem is governed by the Hamiltonian

$$H_{\rm rel}^{\rm free} = -\nabla_{\boldsymbol{r}}^2 + V_{\rm pseudo}, \tag{A1}$$

where, in comparison with Eq. (7), we have suppressed the confinement potential in the Hamiltonian. The scattering states with positive energy, k^2, are solutions everywhere of the eigenvalue problem

$$H_{\rm rel}^{\rm free}\Psi(\boldsymbol{r}) = k^2\Psi(\boldsymbol{r}). \tag{A2}$$

For $kr \gg 1$ the states must have the following form:

$$\Psi_{\boldsymbol{k}}^+(\boldsymbol{r}) \approx e^{i\boldsymbol{k}\cdot\boldsymbol{r}} - f(k,\varphi)\sqrt{\frac{i}{8\pi kr}}\, e^{ikr}, \tag{A3}$$

where $\Psi_{\boldsymbol{k}}^+(\boldsymbol{r})$ is the outgoing wave of momentum $\boldsymbol{k}$, $f(k,\varphi)$ is the scattering amplitude, defined according to the conventions of Ref. 37, and φ is the azimuthal angle. In order to determine the unknow function $f(k,\varphi)$, we parallel Ref. 17 and write the Lippmann-Schwinger equation for $\Psi_{\boldsymbol{k}}^+(\boldsymbol{r})$ in terms of the two-dimensional Green function,

$$\Psi_{\boldsymbol{k}}^+(\boldsymbol{r}) = e^{i\boldsymbol{k}\cdot\boldsymbol{r}} + \int d\boldsymbol{r}' G^+(\boldsymbol{r},\boldsymbol{r}';k^2) V_{\rm pseudo}(\boldsymbol{r}')\Psi_{\boldsymbol{k}}^+(\boldsymbol{r}'). \tag{A4}$$

Here the retarded Green function $G^+(\boldsymbol{r},\boldsymbol{r}';k^2)$ obeys the equation

$$\left(\nabla_{\boldsymbol{r}}^2 + k^2\right) G^+(\boldsymbol{r},\boldsymbol{r}';k^2) = \delta(\boldsymbol{r}-\boldsymbol{r}'), \tag{A5}$$

whose explicit solution is

$$G^+(\boldsymbol{r},\boldsymbol{r}';k^2) = -\frac{i}{4}H_0^{(1)}(k\,|\boldsymbol{r}-\boldsymbol{r}'|), \tag{A6}$$

where $H_0^{(1)}(z)$ is the zero-order Hankel function of the first kind [38]. By replacing G^+ and $V_{\rm pseudo}$ in (A4) with their explicit expressions (A6) and (6), respectively, and then performing the integral over $\boldsymbol{r}'$, one obtains

$$\Psi_{\boldsymbol{k}}^+(\boldsymbol{r}) = e^{i\boldsymbol{k}\cdot\boldsymbol{r}} + \frac{i\pi}{2\log\left(\mathcal{A}a_{\rm 2D}\Lambda\right)}H_0^{(1)}(kr) \times \left[\Psi_{\boldsymbol{k}}^+(\boldsymbol{r}') - \log\left(\mathcal{A}\Lambda r'\right) r'\frac{\partial\Psi_{\boldsymbol{k}}^+(\boldsymbol{r}')}{\partial r'}\right]_{r'\to 0^+}. \tag{A7}$$

As the factor

$$C = \left[\Psi_{\boldsymbol{k}}^+(\boldsymbol{r}') - \log\left(\mathcal{A}\Lambda r'\right) r'\frac{\partial\Psi_{\boldsymbol{k}}^+(\boldsymbol{r}')}{\partial r'}\right]_{r'\to 0^+} \tag{A8}$$

in Eq. (A7) does not depend explicitely on $\boldsymbol{r}$, we find that $\Psi_{\boldsymbol{k}}^+(\boldsymbol{r})$ has the form

$$\Psi_{\boldsymbol{k}}^+(\boldsymbol{r}) = e^{i\boldsymbol{k}\cdot\boldsymbol{r}} + \frac{i\pi C}{2\log\left(\mathcal{A}a_{\rm 2D}\Lambda\right)}H_0^{(1)}(kr). \tag{A9}$$

By inserting Eq. (A9) into (A8) and then by explicitely performing both $\partial/\partial r'$ and $\lim_{r'\to 0^+}$, after some manipulation we obtain an explicit expression for C:

$$C = \frac{\log\left(\mathcal{A}a_{\rm 2D}\Lambda\right)}{\log\left(ka_{\rm 2D}\right)}. \tag{A10}$$

By inserting the above value of C back into Eq. (A9), we obtain an explicit formula for $\Psi_{\boldsymbol{k}}^+(\boldsymbol{r})$ which holds everywhere in space, due to the zero range of the pseudopotential, and that remarkably does not depend on Λ:

$$\Psi_{\boldsymbol{k}}^+(\boldsymbol{r}) = e^{i\boldsymbol{k}\cdot\boldsymbol{r}} + \frac{i\pi}{2\log\left(ka_{\rm 2D}\right)}H_0^{(1)}(kr). \tag{A11}$$

Finally, by using the asymptotic form of the Hankel's function in Eq. (A11),

$$H_0^{(1)}(kr) \approx \sqrt{\frac{2}{\pi kr}}e^{i(kr-\pi/4)} \quad \text{for } kr \gg 1, \tag{A12}$$

we deduce the expression of $f(k,\varphi)$ by direct comparison with Eq. (A3):

$$f(k,\varphi) = -\frac{2\pi}{\log\left(ka_{\rm 2D}\right)}. \tag{A13}$$

The isotropic scattering amplitude (A13) coincides with the exact low-energy limit of $f(k,\varphi)$ for any short-range potential [37]. Therefore, no matter the value of the parameter Λ, the regularized pseudopotential $V_{\rm pseudo}$ correctly reproduces the zero-range features of the true potential.

[1] C. J. Pethick and H. Smith, *Bose-Einstein Condensation in dilute Gases* (Cambridge University Press, Cambridge, 2002).

[2] L. Pitaevskii and S. Stringari, *Bose-Einstein Condensation* (Clarendon Press, Oxford, 2003).

[3] A. J. Leggett, *Quantum Liquids* (Oxford University Press, Oxford, 2006).

[4] For a recent review see I. Bloch, J. Dalibard, and W. Zwerger, Rev. Mod. Phys. **80,** 885 (2008).

[5] M. Rontani, C. Cavazzoni, D. Bellucci, and G. Goldoni, J. Chem. Phys. **124,** 124102 (2006).

[6] K. Huang, *Statistical Mechanics* (Wiley, New York, 1963).

[7] F. A. Berezin and L. D. Fadeev, Dokl. Akad. Nauk SSSR **137,** 1011 (1961); Engl. transl.: Soviet Math. Dokl. **2,** 372 (1961).

[8] R. A. Minlos and L. D. Fadeev, Dokl. Akad. Nauk SSSR **141,** 1335 (1961); Engl. transl.: Soviet Phys. Dokl. **6,** 12 (1961).

[9] S. Adhikari and A. Ghosh, J. Phys. A: Math. Gen. **30,** 6553 (1997).

[10] A. Ghosh, S. Adhikari, and B. Talukdar, Phys. Rev. C **58,** 1913 (1998).

[11] H. E. Camblong and C. R. Ordóñez, Phys. Rev. A **65,** 052123 (2002).

[12] L. Pricoupenko, Phys. Rev. A **73,** 012701 (2006).

[13] A. Sütó, J. Stat. Phys. **109,** 1051 (2002).

[14] T. Busch, B.-G. Englert, K. Rzążewski, and M. Wilkens, Foundations of Physics **28,** 549 (1998).

[15] A. Cabo, J. L. Lucio, and H. Mercado, Am. J. Phys. **66,** Issue 3, 240 (1998).

[16] B. D. Esry and C. H. Greene, Phys. Rev. A **60,** 1451 (1999).

[17] Y. Castin, in *Coherent Atomic Matter Waves,* Lectures Notes of Les Houches Summer School, eds. R. Kaiser, C. Westbrook, and F. David, p. 1-136 (EDP Sciences and Springer-Verlag, Berlin, 2001).

[18] M. Rontani, J. Armstrong, Y. Yu, S. Åberg, and S. M. Reimann, arXiv:0806.3780.

[19] Y. Castin, J. Phys. IV **116,** 87 (2004).

[20] E. Braaten and A. Nieto, Phys. Rev. B **56,** 14745 (1997).

[21] A. Bulgac, J. E. Drut, and P. Magierski, Phys. Rev. Lett. **96,** 090404 (2006).

[22] I. Stetcu, B. R. Barrett, and U. van Kolck, Phys. Lett. B **653,** 358 (2007); I. Stetcu, B. R. Barret, U. van Kolck, and J. P. Vary, Phys. Rev. A **76,** 063613 (2007).

[23] Y. Alhassid, G. F. Bertsch, and L. Fang, Phys. Rev. Lett. **100,** 230401 (2008).

[24] A. Bulgac and Y. Yu, Phys. Rev. Lett. **88,** 042504 (2002).

[25] L. Pricoupenko, Phys. Rev. A **70,** 013601 (2004).

[26] J. von Stecher and C. H. Greene, Phys. Rev. A **75,** 022716 (2007).

[27] S. M. Reimann and M. Manninen, Rev. Mod. Phys. **74,** 1283 (2002).

[28] M. Olshanii and L. Pricoupenko, Phys. Rev. Lett. **88,** 010402 (2002).

[29] Equation (10) actually differs from Eq. (21) of Ref. 14 for a numerical factor which is due to the different definition of a_{2D}. Our usage here is consistent with both the pseudopotential definition (6) and the low-energy expression (A13) for the free-space scattering amplitude.

[30] P. Shea, B. P. van Zyl, and R. K. Bhaduri, arXiv:0807.2979.

[31] J. M. Blatt and V. F. Weisskopf, *Theoretical Nuclear Physics,* Chapt. 11 (Wiley, New York, 1952).

[32] W. Ketterle and M. W. Zwierlein, in *Ultra-cold Fermi Gases,* Eds. M. Inguscio, W. Ketterle, and C. Salomon, International School of Physics Enrico Fermi Vol. 164 (IOS Press, Amsterdam, 2008).

[33] T. Helgaker, P. Jørgensen, and J. Olsen, *Molecular Electronic-structure Theory* (Wiley, Chichester, 2000).

[34] D. S. Petrov, M. Holzmann, and G. V. Shlyapnikov, Phys. Rev. Lett. **84,** 2551 (2000); D. S. Petrov and G. V. Shlyapnikov, Phys. Rev. A **64,** 012706 (2001).

[35] In DONRODRIGO the CI diagonalization is performed over a Hilbert subspace which is eigenstate of both the projection of the total spin and the square total spin itself, S_z and S^2. Such a subspace is built through configurational state functions, which are symmetrized superpositions of Slater determinants. The type of CI diagonalization is "full", namely, all possible Slater determinants built by filling with N particles the Fock-Darwin orbitals are considered. A complete discussion of the method is given in Ref. [5]. See also the code website, www.s3.infm.it/donrodrigo.

[36] Equivalently, here we are neglecting the angular correlation of the ground state, cf. D. Pfannkuche, V. Gudmundsson, and P. A. Maksym, Phys. Rev. B **47,** 2244 (1993).

[37] D. S. Petrov, D. M. Gangardt, and G. V. Shlyapnikov, J. Phys. IV **116,** 5 (2004).

[38] P. M. Morse and H. Feshbach, *Methods of Theoretical Physics* (McGraw-Hill, New York, 1953).